Solvent Effects on Rheological Properties of Polymer Solutions

Yoshinobu Isono* and Mitsuru Nagasawa

Department of Synthetic Chemistry, Nagoya University, Chikusa-ku, Nagoya 464, Japan.
Received November 16, 1979

ABSTRACT: Zero-shear viscosities of poly(α-methylstyrenes) in good and Θ solvents were measured with a capillary viscometer and a Weissenberg rheogoniometer. It was confirmed that the viscosities in good solvents are higher than those in Θ solvents in dilute solutions whereas the opposite is true in concentrated solutions. It is proposed that the reversal is due to the effect of solvent on the interaction strength of entanglement coupling. The strength of entanglement coupling is discussed in terms of the network-rupture model.

The rheological properties of polymer solutions or melt in the linear region of deformation can be expressed by two parameters,[1,2] for example, the zero-shear viscosity η^0 and the steady-state compliance J_e. The former is a measure of energy dissipation and the latter is a measure of energy storage. A number of experimental studies have accumulated on the effect of solvent on viscosity,[3-11a] and recently a few papers have been published on the solvent effect on steady-state compliance.[11a,12] Together these clearly show the following. In dilute or moderately concentrated solution (the so-called Rouse region), (a) the specific viscosity in a poor solvent is lower than that in a good solvent and (b) the steady-state compliance in a poor solvent is higher than that in a good solvent. On the other hand, in concentrated solution (the so-called network region), (c) the specific viscosity in a poor solvent is higher than that in a good solvent (or identical in both solvents[11b]) and (d) the steady-state compliance in both good and poor solvents coincide with each other. It is clear both experimentally and theoretically that fact a is due to the polymer's larger radius of gyration in a good solvent than in a poor solvent. At present, however, facts b–d have not fully been explained.

If a quasi-network is formed in concentrated solutions, the steady-state compliance may be determined by the molecular weight for adjacent entanglement coupling, i.e., by the density of entanglement coupling only. Fact d, therefore, means that the density of entanglement coupling is independent of the nature of solvent. On the other hand, it is generally believed that the viscosity is determined by two factors, namely, the radius of gyration of polymer molecule and the density of entanglement coupling.[1,2] However, these two factors are not enough to explain fact c, if there is no difference in the densities of entanglement coupling in good and poor solvents. Moreover, it was reported[13-16] that the radius of gyration of polymer in a good solvent is comparable to that in a Θ solvent (i.e., poor solvent) in concentrated solutions. To explain fact c, therefore, we predict that there must be a difference between the strength of entanglement coupling in a good solvent and that in a poor solvent.

The purpose of this work is to confirm facts b–d experimentally and to present an idea concerning the strength of entanglement coupling to explain the solvent effect on viscosity. The idea can be supported by the so-called stress overshoot experiments if we employ the network-rupture model[17] in transient stress phenomena.

Experimental Section

Samples. Poly(α-methylstyrenes) having narrow molecular weight distributions used in this work were prepared by an anionic polymerization method.[18] Low and high molecular weight tails were removed by fractional precipitation from benzene solution with addition of methanol. These samples are the same as used in previous works.[11a,19] The molecular weights of samples used are listed in Table I. These values were determined by light scattering or osmometry in a previous work.[20]

Table I
Samples

sample no.	$10^{-6}M_w$	sample no.	$10^{-6}M_w$
α-19A	1.6_5	α-004	0.33_2
α-20	1.1_2	α-002	0.14_6
α-005	0.44_0		

Table II
Solvents

solvent	T, °C	η_s, cP	d, g/mL	Θ point, °C
toluene	30	0.522	0.8565	*a*
α-chloronaphthalene	50	1.65	1.168	*a*
trans-decalin	30	1.76	0.8627	9.5
n-butylbenzyl phthalate	50	15.5	1.096	46

[a] Good solvent.

Solvents. Toluene and α-chloronaphthalene were used as good solvents. First grade toluene and special grade α-chloronaphthalene of Katayama Chemical Co. were purified by the procedure described in previous papers.[11a,20]

trans-Decalin and *n*-butylbenzyl phthalate were used as Θ solvents. The former, purified by a procedure described in a previous paper,[20] had a gas chromatographic purity greater than 99.8%. The Θ temperature of *trans*-decalin is 9.5 °C.[20] Purification of *n*-butylbenzyl phthalate was carried out by distillation under 10^{-4} mmHg at about 160 °C. The Θ temperature of *n*-butylbenzyl phthalate was determined by the Schultz–Flory method,[21] as shown in Figure 1. In Figure 1, T_c is the critical precipitation temperature. The Θ temperature of *n*-butylbenzyl phthlate is about 46 °C.

The densities, the viscosities, and the Θ temperatures of the solvents used in this work are listed in Table II.

Measurements. Zero-shear viscosities of toluene and *trans*-decalin solutions of poly(α-methylstyrenes) were measured at 30 °C with an accuracy of ±0.1 °C by a capillary viscometer with a continuously variable pressure head designed by Maron, Krieger, and Sisko.[22] Four capillaries having different diameters were used. The method of measurement and the dimensions of the other parts were nearly identical with those described by Maron et al.[22] The viscosity η was calculated by eq 1, where h is the height of the

$$\eta = -\frac{1}{B}\frac{\mathrm{d}(\log h)}{\mathrm{d}t} \tag{1}$$

mercury manometer from its equilibrium position, t is time, and B is the apparatus constant. In this measurement, $\mathrm{d}(\log h)/\mathrm{d}t$ was constant, confirming the Newtonian flow.

The measurement of the primary normal stress difference and shear stress of α-chloronaphthalene and *n*-butylbenzyl phthalate solutions of poly(α-methylstyrenes) was carried out with a Type R-17 Weissenberg rheogoniometer manufactured by Sangamo Controls Ltd. and equipped with a gap-servo system. The details and reliability of the Type R-17 Weissenberg rheogoniometer in

0024-9297/80/2213-0862$01.00/0

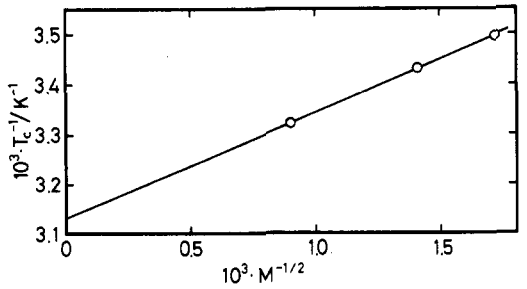

Figure 1. Determination of the Θ temperature for poly(α-methylstyrene) in *n*-butylbenzyl phthalate. Molecular weights of the samples, from left to right, are 1.24×10^6, 0.506×10^6, and 0.340×10^6.

the present experimental range were confirmed by the method reported in previous papers.[23,24] The cone and plate had a 5-cm and 4° angle. The experiments with the rheogoniometer were carried out at 50 °C with an accuracy of ±0.1 °C. The values of shear stress were continuously recorded on an electromagnetic recorder. The viscosity coefficient $\eta(\dot{\gamma})$ and the primary normal stress difference coefficient $\psi_{12}(\dot{\gamma})$ are calculated as $P_{12}/\dot{\gamma}$ and $(P_{11} - P_{22})/\dot{\gamma}^2$, respectively, where P_{12} is the shear stress, $P_{11} - P_{22}$ is the primary normal stress difference, measured with the Weissenberg rheogoniometer, and $\dot{\gamma}$ is the shear rate. The zero-shear viscosity η^0 and zero-shear primary normal stress difference coefficient $\psi_{12}{}^0$ were determined by extrapolation to zero-shear rate. The steady-state compliance J_e can be determined by extrapolating the apparent steady-state compliance J_s calculated from eq 2 to zero-shear rate.

$$J_s = (P_{11} - P_{22})/2P_{12}{}^2 \tag{2}$$

Solutions of about 10–40 g/dL were first prepared by mixing weighed amounts of polymer and the solvent at 50 °C. To accelerate the dissolution of polymer, a considerable amount of cyclohexane was added to the mixture. The mixtures were gently stirred three times a day by hand until the solution became uniform. Cyclohexane was removed by evaporation in a vacuum oven at 50 °C. Dilution was carried out by weight. Polymer concentrations were converted to g/dL, assuming the additivity of specific volumes of polymer and solvent. In measurements with *n*-butylbenzyl phthalate solutions, both the solution and the cone–plate were held at a temperature about 5–10 °C higher than the experimental temperature and then gradually lowered to the experimental temperature. Experiments were started 20 min after the experimental temperature was attained. When measurements were done repeatedly with a sample solution, the solution was kept at rest at least for 30 min before measurement, and it was confirmed that the zero-shear viscosity of the solution observed agreed with the initial value.

Results

(A) Polymer Concentration Dependence of η^0 and J_e in Good and Θ Solvents. The observed values of zero-shear specific viscosity $\eta_{sp}{}^0$ of poly(α-methylstyrenes) both in toluene (good solvent) and in *trans*-decalin (Θ solvent, $T_\Theta = 9.5$ °C) are double-logarithmically plotted against polymer concentration C (g/dL) in Figure 2, where $\eta_{sp}{}^0$ is defined by $\eta_{sp}{}^0 = (\eta^0 - v_s\eta_s{}^0)/\eta_s{}^0$ and v_s is the volume fraction of solvent. In this figure, it is clear that fact c described in the introduction holds for ordinary solvents such as toluene and *trans*-decalin. Numerical data for η^0 of poly(α-methylstyrenes) in toluene and *trans*-decalin are listed in Table III.

Typical plots of log $\eta(\dot{\gamma})$ vs. log $\dot{\gamma}$ for α-chloronaphthalene solutions of sample α-19A are shown in Figure 3A. Examples of ψ_{12} and J_s double-logarithmically plotted against $\dot{\gamma}$ are shown in Figure 4. If the data in Figure 3A are replotted in the form of reduced viscosity log $\eta(\dot{\gamma})/\eta^0$ vs. log $\dot{\gamma}\eta^0/C^2$, all data form a single curve as shown in Figure 3B. The plot in Figure 3B has the same meaning as the plot of Berry,[25,26] i.e., log $\eta(\dot{\gamma})/\eta^0$ vs. log $\eta^0 J_e\dot{\gamma}$. In

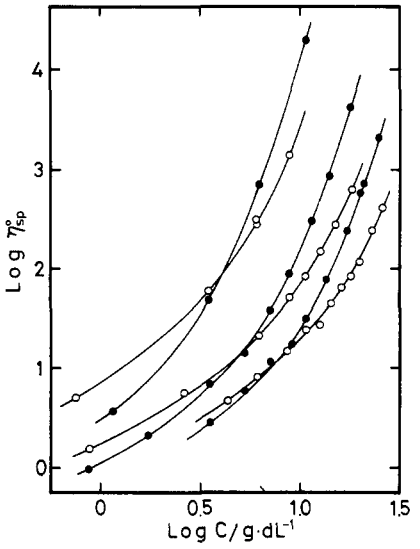

Figure 2. Polymer concentration dependence of $\eta_{sp}{}^0$ in toluene (○) and in *trans*-decalin (●) at 30 °C. Samples, from top to bottom, are α-20, α-004, and α-002.

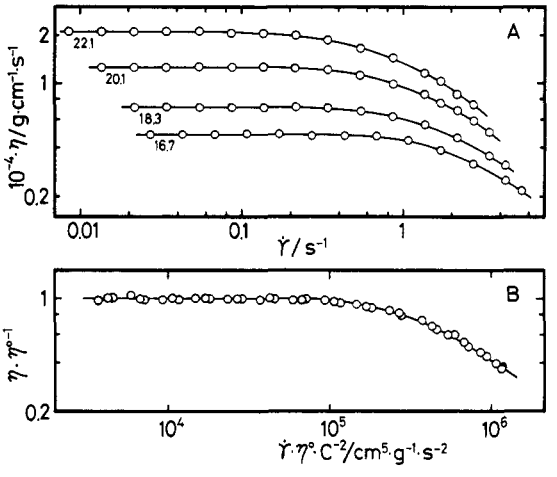

Figure 3. (A) Double-logarithmic plots of $\eta(\dot{\gamma})$ vs. $\dot{\gamma}$ for α-19A in α-chloronaphthalene at 50 °C. Concentrations (g/dL) are as shown in the figure. (B) Double-logarithmic plot of $\eta(\dot{\gamma})/\eta^0$ vs. $\eta^0\dot{\gamma}/C^2$ for the data in A.

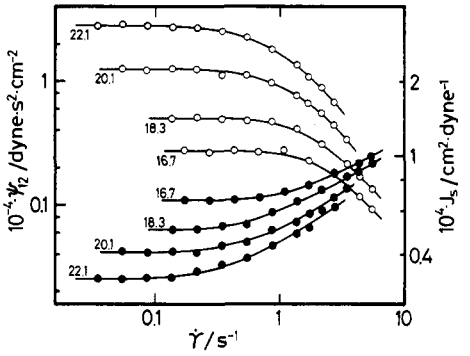

Figure 4. Double-logarithmic plots of $\psi_{12}(\dot{\gamma})$ (○) and J_s (●) vs. $\dot{\gamma}$ for α-19A. Concentrations are the same as those in Figure 3.

Figure 3B, moreover, the solid line shows the calculated values of Graessley (eq 3),[25] horizontally shifted to be superposed on the curve.

$$\eta(\dot{\gamma})/\eta^0 = g(\theta)^{3/2}h(\theta) \tag{3}$$

$$g(\theta) = (2/\pi)[\cot^{-1}\theta + \theta/(1 + \theta^2)] \tag{4}$$

$$h(\theta) = (2/\pi)[\cot^{-1}\theta + \theta(1 - \theta^2)/(1 + \theta^2)^2] \tag{5}$$

$$\theta = \dot{\gamma}\tau/2 \tag{6}$$

Table III
Zero-Shear Viscosity

sample no.	solvent	T,[a] °C	C, g/dL	η^0, P
α-20	toluene	30	8.75	7.43×10^0
			6.05	1.48×10^0
			5.98	1.64×10^0
			3.46	3.15×10^{-1}
			0.75	3.11×10^{-2}
α-004	toluene	30	18.3	3.30×10^0
			15.1	1.46×10^0
			12.6	7.84×10^{-1}
			10.6	4.43×10^{-1}
			8.87	2.79×10^{-1}
			6.13	1.14×10^{-1}
			2.60	3.46×10^{-2}
			0.88	1.33×10^{-2}
α-002	toluene	30	26.0	2.18×10^0
			23.0	1.26×10^0
			19.9	6.14×10^{-1}
			18.1	4.44×10^{-1}
			16.1	3.39×10^{-1}
			14.3	2.38×10^{-1}
			12.4	1.46×10^{-1}
			10.7	1.30×10^{-1}
			8.53	8.24×10^{-2}
			6.05	4.66×10^{-2}
			4.31	2.93×10^{-2}
α-20	*trans*-decalin	30	10.7	3.46×10^2
			6.17	1.25×10
			3.47	8.73×10^{-1}
			1.15	8.30×10^{-2}
α-004	*trans*-decalin	30	17.8	7.53×10
			14.1	1.52×10
			11.4	5.26×10^0
			8.81	1.58×10^0
			7.04	6.80×10^{-1}
			5.23	2.64×10^{-1}
			3.48	1.38×10^{-1}
			1.73	5.42×10^{-2}
			0.87	3.46×10^{-2}
α-002	*trans*-decalin	30	24.8	3.72×10
			20.9	1.29×10
			20.0	1.04×10
			17.1	4.30×10^0
			13.5	1.39×10^0
			10.6	5.57×10^{-1}
			9.00	3.26×10^{-1}
			7.04	2.19×10^{-1}
			5.25	1.20×10^{-1}
			3.50	6.65×10^{-2}

[a] ±0.1 °C.

The plots of log $\eta_{sp}{}^0$ of poly(α-methylstyrenes) both in α-chloronaphthalene (good solvent) and in *n*-butylbenzyl phthalate (Θ solvent, T_Θ = 46 °C) vs. log C are shown in Figure 5. Some of the data in Figure 5 for sample α-005 in α-chloronaphthalene have already been reported by Sakai et al.[19] Previously reported[11] values of $\eta_{sp}{}^0$ for sample α-005 in a different Θ solvent, *n*-undecyl anisitate (T_Θ = 33 °C, η_s = 10.7 cP), at 40 °C are also plotted in Figure 5. It is clear that the agreement of $\eta_{sp}{}^0$ in the two different Θ solvents is satisfactory. In this figure, too, the crossing of the two curves in good and Θ solvents is observed at $C \simeq$ 3.4–4.2 g/dL. From Figures 2 and 5, it is certain that $\eta_{sp}{}^0$ in good solvents is higher at lower concentrations but lower at higher concentrations than that in Θ solvents. These results are in accord with the results reported by several authors.[3-11a]

The observed values of steady-state compliance J_e are double-logarithmically plotted against C in Figure 6. Some of the data in Figure 6 for sample α-005 in α-chloronaphthalene have already been reported by Sakai et al.[19]

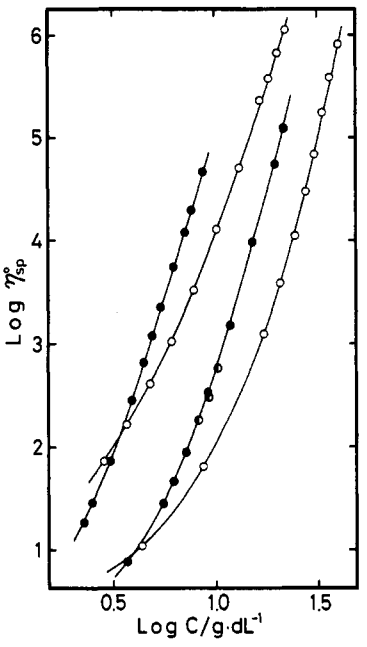

Figure 5. Polymer concentration dependence of $\eta_{sp}{}^0$ of poly(α-methylstyrenes) in α-chloronaphthalene (○) and *n*-butylbenzyl phthalate (●) at 50 °C. Samples are, from top to bottom, α-19A and α-005. ◐ shows the data for α-005 in *n*-undecyl anisitate at 40 °C.[11]

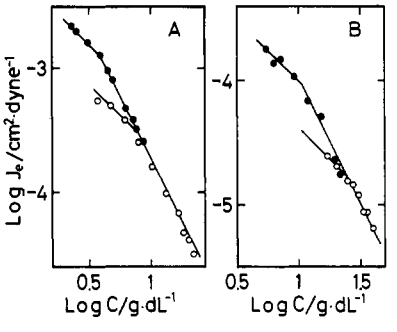

Figure 6. Polymer concentration dependence of J_e of poly(α-methylstyrenes) in α-chloronaphthalene (○) and *n*-butylbenzyl phthalate (●) at 50 °C: (A) sample α-19A; (B) sample α-005.

In the higher concentration region, no difference is observed between J_e in good and Θ solvents, whereas in the moderately concentrated solution (the Rouse region), J_e in the Θ solvent is higher than that in the good solvent. These results are in accord with previous conclusions.[11a,12] Numerical data of η^0 and J_e for poly(α-methylstyrenes) in α-chloronaphthalene and *n*-butylbenzyl phthalate are listed in Table IV.

(B) Determination of the Rupture Energy of an Entanglement Coupling. Examples of the shear stress developments after onset of steady shear flow are shown in Figure 7. The apparent viscosity coefficient $\eta^d(t|\dot{\gamma})$ is defined by $\eta^d(t|\dot{\gamma}) = P_{12}{}^d(t|\dot{\gamma})/\dot{\gamma}$, where $P_{12}{}^d(t|\dot{\gamma})$ is the shear stress development under a shear rate $\dot{\gamma}$ in the polymer solution at time t. The experimental points in Figure 7 simply denote the points selected for converting the continuously recorded values into apparent viscosities. These curves have the same qualitative features as those reported previously.[17] The uppermost curve shows the stress development in the linear region. The curves at finite shear rates coincide with the uppermost curve at the initial state and deviate from the uppermost curve after certain times.

If we employ the network-rupture model of Kajiura et al., the work (ΔW) to transform the entangled structure

Table IV
Steady-Flow Viscosity and Compliance at Zero-Shear Rate

sample no.	solvent	T,[a] °C	C, g/dL	η^0, P	J_e, cm²/dyn
α-19A	α-chloronaphthalene	50	22.1	2.11×10^4	3.17×10^{-5}
			20.1	1.27×10^4	4.07×10^{-5}
			18.3	7.13×10^3	4.74×10^{-5}
			16.7	4.70×10^3	6.09×10^{-5}
			13.2	9.55×10^2	9.77×10^{-5}
			10.2	2.42×10^2	1.60×10^{-4}
			7.87	6.22×10	2.54×10^{-4}
			6.12	2.00×10	3.86×10^{-4}
			4.76	7.71×10^0	5.04×10^{-4}
			3.69	3.16×10^0	5.55×10^{-4}
			2.87	1.40×10^0	
α-005	α-chloronaphthalene	50	40.0	1.54×10^4	6.50×10^{-6}
			36.2	7.34×10^3	8.80×10^{-6}
α-19A	*n*-butylbenzyl phthalate	50	8.72	7.07×10^3	2.57×10^{-4}
			7.67	3.08×10^3	3.12×10^{-4}
			7.13	1.83×10^3	3.91×10^{-4}
			6.23	8.47×10^2	4.77×10^{-4}
			4.92	1.84×10^2	8.19×10^{-4}
			4.48	1.02×10^2	9.57×10^{-4}
			3.92	4.30×10	1.28×10^{-3}
			3.07	1.13×10	1.65×10^{-3}
			2.51	4.39×10^0	2.02×10^{-3}
			2.29	2.90×10^0	2.20×10^{-3}
α-005	*n*-butylbenzyl phthalate	50	21.7	1.89×10^4	1.75×10^{-5}
			19.6	8.42×10^3	2.29×10^{-5}
			15.2	1.46×10^3	5.15×10^{-5}
			11.9	2.29×10^2	6.86×10^{-5}
			9.18	5.18×10	1.07×10^{-4}
			7.14	1.38×10	1.49×10^{-4}
			6.24	7.36×10^0	1.36×10^{-4}
			5.51	4.53×10^0	1.79×10^{-4}
			3.72	1.33×10^0	

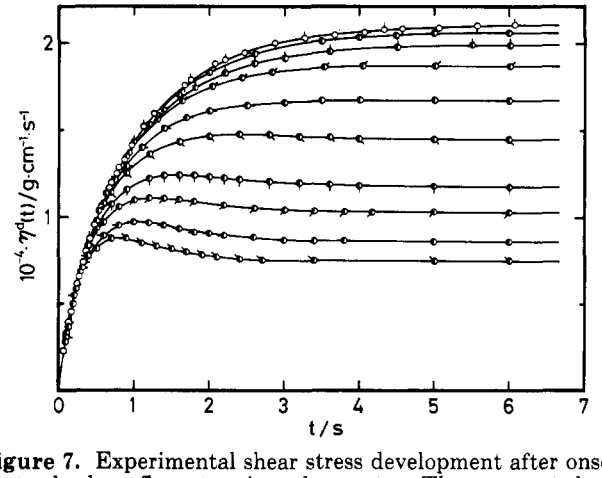

Figure 7. Experimental shear stress development after onset of steady shear flow at various shear rates. The apparent shear viscosity coefficient $\eta^d(t)$ is related to the shear stress $P_{12}^d(t)$ by $P_{12}^d(t) = \eta^d(t)\dot{\gamma}$. The sample is α-19A in α-chloronaphthalene at 50 °C and the concentration is 22.1 g/dL. $\dot{\gamma}$ shear rates: (○) 0.0216; (○) 0.0342; (○) 0.0544; (◐) 0.136; (◐) 0.216; (◐) 0.342; (◐) 0.544; (◐) 0.861; (◐) 1.36; (◐) 1.71; (◐) 2.16; (◐) 2.73 s^{-1}. The zero-shear viscosity of this sample solution is 2.11×10^4 P. Circles denote the points selected for converting the observed values into the apparent viscosity coefficient (see text).

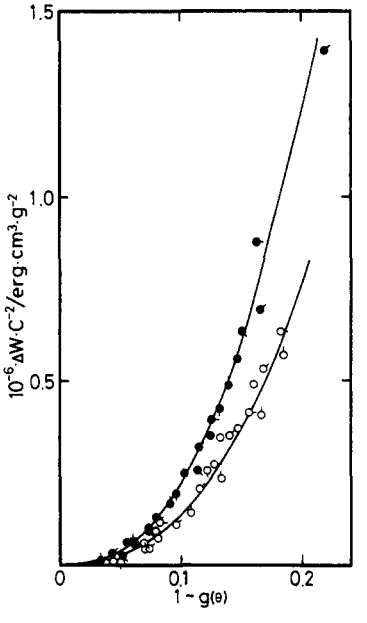

Figure 8. Plots of $\Delta W/C^2$ vs. $1 - g(\theta)$ for poly(α-methylstyrenes) in α-chloronaphthalene (○) and *n*-butylbenzyl phthalate (●) at 50 °C. ○ and ● show the data for α-005 at 40.0 and 21.7 g/dL, respectively. ○, ○, ○ and ○ show the data for α-19A at 22.1, 20.1, 18.3, and 16.7 g/dL, respectively. ●, ●, ●, ●, and ● show the data for α-19A at 8.72, 7.67, 7.13, 6.23, and 4.92 g/dL, respectively.

from that at the equilibrium state to that at the steady state with shear rate $\dot{\gamma}$ is given by [17]

$$\Delta W = \dot{\gamma}^2\left[\int_0^{t_s} \eta^d(t|\dot{\gamma})\, dt - t_s\eta(\infty|\dot{\gamma}) + \tfrac{1}{2}\psi_{12}(\infty|\dot{\gamma})\right] \quad (7)$$

where $\eta^d(t|\dot{\gamma})$ is the apparent viscosity at time t in the stress development under the shear rate $\dot{\gamma}$, $\eta(\infty|\dot{\gamma})$ and $\psi_{12}(\infty|\dot{\gamma})$ are the viscosity and primary normal stress difference coefficient at the steady state under the shear rate $\dot{\gamma}$, respectively, and t_s is a time after the stresses reach the steady-state values. Since the density of entanglement coupling in concentrated solutions in which the quasi-network structure is formed is proportional to C^2, $\Delta W/C^2$ may be proportional to the rupture energy of entanglement coupling per unit number of entanglement coupling.

According to the theory of Graessley,[27] the fractional reduction of the entanglement density $[1 - g(\theta)]$ can be estimated from eq 4. Figure 8 shows the relationship between $\Delta W/C^2$ and $1 - g(\theta)$. It can be observed in Figure

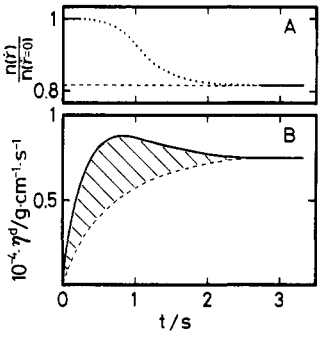

Figure 9. Diagrams for explaining a transition from the equilibrium-entangled structure to the steady-state entangled structure at $\dot{\gamma}$. (A) Thick solid lines denote the reduced entanglement density $n(\dot{\gamma})/n(\dot{\gamma}=0)$ for α-19A in α-chloronaphthalene at 22.1 g/dL at the equilibrium state ($\dot{\gamma}$ = 0) (left) and at steady state with shear rate $\dot{\gamma}$ = 2.73 s^{-1} (right). The dotted line denotes a schematic graph of the change in the reduced entanglement density with time. (B) The solid line shows the apparent shear viscosity at $\dot{\gamma}$ = 2.73 s^{-1} corresponding to the change in entanglement density shown in A. The broken line shows an apparent shear stress development in a solution with an imaginary constant entanglement density as shown by the broken line in A.

8 that the rupture energy of entanglement coupling becomes higher as the fractional reduction of the entanglement density becomes larger and also that the value of $\Delta W/C^2$ is higher in a Θ solvent than in a good solvent. We point out that the value of $\Delta W/C^2$ is independent of molecular weight in both solvents.

Discussion

Figure 7 as well as previous data[11a] clearly shows that the steady-state compliances J_e in good and poor solvents agree with each other and are proportional to the inverse square polymer concentration C^{-2} if the polymer concentration is higher than a critical value. Therefore, it can be concluded that a quasi-network is formed in these solutions and, moreover, that the densities of entanglement coupling in good and poor solvents are equal. In addition to the data in the literature,[3-11a] the present data (Figures 2 and 5) also show that the specific viscosity of the polymer solutions in poor solvents is lower than that in good solvents in dilute solutions, whereas in concentrated solutions the opposite is true. Neither the difference in the radius of gyration nor that in the density of entanglement coupling can be the reason for the reversal of $\eta_{sp}{}^0$ in concentrated solutions. The radius of gyration in good solvents may decrease with concentration, but it is unlikely that the radius of gyration is smaller in good solvents than in poor solvents in concentrated solutions. The reversal of $\eta_{sp}{}^0$ is generally found in the concentration range where both values of radius of gyration in good and poor solvents become almost identical.[13-16] Our explanation for this phenomenon is that the strength of entanglement coupling is larger in a poor solvent than in a good solvent. This explanation seems to be reasonable if we consider the excluded-volume effect acting between segments in dilute solutions. A stronger apparent repulsive force must act between segments in good solvents than in poor solvents. If the solvent power decreases below the Θ point, the segments apparently attract each other so that the polymer solution may show phase separation in dilute solutions or may become like a gel in concentrated solutions. Williams et al.[7] explained this solvent effect in terms of the polymer aggregation in poor solvents. Vinogradov et al.[10] explained it in terms of the difference of glass transition temperature of polymer solutions in different solvents.

Figure 3B as well as the experimental data in the literature[2] shows that the shear rate dependence of shear viscosity of polymer solutions can quantitatively be explained by the theory of Graessley,[27] in which only the decrease in the entanglement density with shear rate is taken into account. If we follow the theory of Graessley, the entanglement density at the final state with shear rate $\dot{\gamma}$ must be different from that at the initial state in Figure 7. During the stress development, the entanglement density must be changed from the initial value to the steady value. In Figure 9A, the difference between the entanglement density at the initial state and at the steady state in a stress development experiment ($\dot{\gamma}$ = 2.73 s^{-1}) is exemplified by the horizontal solid line. The change in the entanglement density with time is also schematically shown by a dotted line in the figure. In correspondence to this change in the entanglement density, a change in the apparent shear viscosity with time may be observed as shown in Figure 9B.[17] A broken line in Figure 9B is schematically drawn, assuming that it would be observed if the entanglement density were kept at constant $[\eta(\dot{\gamma})/\eta(\dot{\gamma} = 0) = 0.816]$.

The shear stress overshoot phenomena can be expressed by various theories besides the present network-rupture model, for example, by using the so-called rate-dependent-type or strain-dependent-type of constitutive equations, without assuming the change in density of entanglement coupling with shear rate.[28] Since, in particular, the latter theory can explain the phenomena at least qualitatively, the present network-rupture model may be considered to be an assumption at present. If we accept this, however, the strength of entanglement coupling can be estimated experimentally. That is, if the network-rupture model is acceptable and if the contribution of the other kind of energy dissipation during the transition of entangled structure is negligible compared with the energy dissipation due to entanglement coupling, the work to change the density of entanglement coupling from the equilibrium value to the steady-state value at the shear rate $\dot{\gamma}$ is given by the shaded area in Figure 9B. The area can be analytically calculated with eq 7.

Figure 8 clearly shows that, to disentangle an entanglement coupling, more energy is required in a poor solvent than in a good solvent. That is, the strength of entanglement coupling in a poor solvent is higher than that in a good solvent. Therefore, it may be concluded that the higher specific viscosity of polymer concentrated solution in a poor solvent than in a good solvent is caused by the higher strength of entanglement coupling in a poor solvent than in a good solvent. Measurements of entanglement rupture energy in the other polymer solutions in reference to the reversal phenomenon of $\eta_{sp}{}^0$ have not been carried out. However, we know from our experience that the stress overshoot phenomena can be observed more easily in poor solvents than in good solvents.

Finally, fact b, i.e., the fact that J_e in a poor solvent in the Rouse region is higher than in a good solvent, is equivalent to the fact that the critical concentration $C_c{}^J$ in the relation between J_e and C is lower in a poor solvent than in a good solvent. That is, a quasi-network can be formed in a poor solvent more easily than in a good solvent. This is in agreement with the present model in discussing viscosity.

Acknowledgment. We thank Mr. Shinji Katagai for his assistance in measuring the zero-shear viscosity of the sample with the Maron–Krieger–Sisko type viscometer.

References and Notes

(1) J. D. Ferry, "Viscoelastic Properties of Polymers", 2nd ed., Wiley, New York, 1970.
(2) W. W. Graessley, *Adv. Polym. Sci.*, **16**, 1 (1974).

(3) J. D. Ferry, E. L. Foster, G. V. Browning, and W. M. Sawyer, *J. Colloid Sci.*, **6**, 377 (1951).
(4) M. F. Johnson, W. W. Evans, I. Jordan, and J. D. Ferry, *J. Colloid Sci.*, **7**, 498 (1952).
(5) J. D. Ferry, L. D. Grandine, Jr., and D. C. Udy, *J. Colloid Sci.*, **8**, 529 (1953).
(6) S. Onogi, S. Kimura, T. Kato, T. Masuda, and N. Miyanaga, *J. Polym. Sci., Part C*, **15**, 381 (1966).
(7) K. S. Gandhi and M. C. Williams, *J. Polym. Sci., Part C*, **35**, 211 (1971).
(8) K. S. Gandhi and M. C. Williams, *J. Appl. Polym. Sci.*, **16**, 2721 (1972).
(9) O. Quadrat and J. Podnecká, *Collect. Czech. Chem. Commun.*, **37**, 2402 (1972).
(10) V. E. Dreval, A. Ya. Malkin, and G. V. Vinogradov, *Eur. Polym. J.*, **9**, 85 (1973).
(11) (a) H. Kajiura, Y. Ushiyama, T. Fujimoto, and M. Nagasawa, *Macromolecules*, **11**, 894 (1978); (b) G. C. Berry, H. Nakayasu, and T. G. Fox, *J. Polym. Sci., Polym. Phys. Ed.*, **17**, 1825 (1979).
(12) Y. Isono, T. Fujimoto, H. Kajiura, and M. Nagasawa, *Polym. J.*, **12**, 363 (1980).
(13) J. P. Cotton, D. Decker, H. Benoit, B. Farnoux, J. Higgins, G. Jannink, R. Ober, C. Picot, and J. des Cloizeaux, *Macromolecules*, **7**, 863 (1974).
(14) M. Daoud, J. P. Cotton, B. Farnoux, G. Jannink, G. Sarma, H. Benoit, R. Duplessix, C. Picot, and P. G. de Gennes, *Macromolecules*, **8**, 804 (1975).
(15) H. Hayashi, F. Hamada, and A. Nakajima, *Makromol. Chem.*, **178**, 827 (1977).
(16) H. Hayashi, F. Hamada, and A. Nakajima, *Polymer*, **18**, 638 (1977).
(17) H. Kajiura, M. Sakai, and M. Nagasawa, *Trans. Soc. Rheol.*, **20**, 575 (1976).
(18) T. Fujimoto, N. Ozaki, and M. Nagasawa, *J. Polym. Sci., Part A-2*, **6**, 129 (1968).
(19) M. Sakai, T. Fujimoto, and M. Nagasawa, *Macromolecules*, **5**, 786 (1972).
(20) T. Kato, K. Miyaso, I. Noda, T. Fujimoto, and M. Nagasawa, *Macromolecules*, **3**, 777 (1970).
(21) A. R. Schultz and P. J. Flory, *J. Am. Chem. Soc.*, **74**, 4760 (1952).
(22) S. H. Maron, I. M. Krieger, and A. W. Sisko, *J. Appl. Phys.*, **25**, 971 (1954).
(23) H. Endo and M. Nagasawa, *J. Polym. Sci., Part A-2*, **8**, 371 (1970).
(24) H. Kajiura, H. Endo, and M. Nagasawa, *J. Polym. Sci., Polym. Phys. Ed.*, **11**, 2371 (1973).
(25) G. C. Berry, *J. Chem. Phys.*, **46**, 1338 (1967).
(26) G. C. Berry, B. L. Hager, and C. P. Wong, *Macromolecules*, **10**, 361 (1977).
(27) W. W. Graessley, *J. Chem. Phys.*, **43**, 2696 (1965); **47**, 1942 (1967).
(28) Y. Isono, H. Kajiura, and M. Nagasawa, *J. Rheol.*, **23**, 79 (1979).

Rheooptical Studies of Racemic Poly(γ-benzyl glutamate) Liquid Crystals

Tadahiro Asada,* Hiromochi Muramatsu, Ryoji Watanabe, and Shigeharu Onogi

Department of Polymer Chemistry, Kyoto University, Kyoto 606, Japan.
Received June 21, 1979

ABSTRACT: Both the rheooptical and rheological properties of a polymer liquid crystalline system may well be interpreted by supposing three typical structural models for the bulk structure of the system: (1) a piled polydomain, in which many small domains are piled randomly; (2) a dispersed polydomain, in which a large domain occupies the whole volume, but not without the presence of some smaller domains; (3) a monodomain continuous phase. The piled polydomain which is usually seen for a virgin sample is considered to be transformed finally into a monodomain continuous phase by a shear or other external field. The flow properties of concentrated solutions of racemic poly(γ-benzyl glutamate) in *m*-cresol at concentrations above the *B* point have been observed with a rheometer equipped with a quartz cone-plate and the transmitted light intensities (I_x, $I_\parallel$, I_E) of polarized light have been simultaneously measured as a function of shear rate.

Studies[1-8] of the rheological behavior of polymer liquid crystals provide a great deal of technologically important information, particularly information about the ability to spin such materials into fibers, but rheological methods alone cannot give the full picture. Such materials form complicated and unstable superstructures and accompanying unusual textures. Therefore, new rheooptical techniques were developed in our laboratory for studying the relation between structure and rheological properties of various liquid crystals.[9-12] This paper is concerned with the rheooptical properties of solutions of poly(γ-benzyl glutamate) in the liquid-crystal state.

Experimental Section

Measurements. A block diagram of one of the rheooptical instruments (apparatus II) is shown in Figure 1. A cone and plate type rheometer equipped with a transparent cone and plate made of quartz is combined with the optical system. A monochromatic laser light beam (λ = 6328 Å) passes through a polarizer (P), quartz plate (E), sample (F), quartz cone (G), and analyzer (A). The transmitted light is finally detected by a photomultiplier tube (PM_l). Thus, the apparatus enables us to simultaneously measure rheological properties and transmission of polarized lights through a sheared sample. The diameters of the cones and plates employed were kept constant (8 cm). Four cones of different cone angles (0.865, 1.01, 2.06, 3.85°) were used.

At room temperature (22 °C), the shear stress and transmitted light intensities (I_x, $I_\parallel$, I_E) were measured simultaneously as functions of shear rate (3×10^{-2}–2×10^2 s^{-1}), where I_x, $I_\parallel$, and I_E are fractional transmitted light intensities when crossed polarizers (at ψ = 45° in Figure 2), parallel polarizers (at ψ = 45°), and crossed polarizers at the extinction position (at ψ = 0°) are used, respectively. The geometries are shown in Figure 2.

Although it depended on concentration and shear rate whether or not the optical quantities varied with time at constant shear rate, all data presented here were taken at the steady state, and these were confirmed by observing for a much longer time than that required for recognizing the steady state of the stress: for example, 60 min at $\dot{\gamma} = 3.47 \times 10^{-2}$ s^{-1}, 30 min at $\dot{\gamma} = 6.9 \times 10^{-1}$ s^{-1}, and 1 min at $\dot{\gamma} = 1.04 \times 10^2$ s^{-1}.

Materials. Poly(γ-benzyl L-glutamate) of weight-average molecular weight 15×10^4 and poly(γ-benzyl D-glutamate) of weight-average molecular weight 15×10^4 were obtained from Sigma Chemical Co. These weight-average molecular weights $\bar{M}_w$ were estimated from the intrinsic viscosity [η] of dilute solutions in dichloroacetic acid at 25 °C, using the relation proposed by Doty et al.[13] Equal amounts of both materials were dissolved in

0024-9297/80/2213-0867$01.00/0